Precipitation and Soil Moisture Datasets Show Severe Droughts in the MENA Region

Ahmad Al Bitar, Sami Najem, Lionel Jarlan, Mehrez Zribi, Ghaleb Faour

Precipitation and Soil Moisture Datasets Show Severe Droughts in the MENA Region

Ahmad Al Bitar (ahmad.albitar@cesbio.cnes.fr)
Centre d'Etudes Spatiales de la BIOsphère
Sami Najem
National Council for Scientific Research
Lionel Jarlan
Centre d'Etudes Spatiales de la BIOsphère
Mehrez Zribi
Centre d'Etudes Spatiales de la BIOsphère
Ghaleb Faour
National Council for Scientific Research

Research Article

Keywords: MENA, ERA5, TRMM, ECMWF

Posted Date: January 14th, 2021

DOI: https://doi.org/10.21203/rs.3.rs-141859/v1

Precipitation and soil moisture datasets show severe droughts in the MENA region

Ahmad Al Bitar[1,*], Sami Najem[2], Lionel Jarlan[1], Mehrez Zribi[1], and Ghaleb Faour[2]

[1]CESBIO, Université de Toulouse, CNES, CNRS, IRD, INRAe, UPS, 18 avenue Edouard Belin, 31401 Toulouse, France
[2]National Center for Remote Sensing, National Council for Scientific Research (CNRS), Riad Al Soloh, 1107 2260, Beirut, Lebanon
[*]ahmad.albitar@cesbio.cnes.fr

ABSTRACT

The Middle East and North Africa (MENA) region is facing the challenge of lingering droughts. Precipitation and soil moisture are two Essential Climate Variables (ECVs) that are relevant for drought monitoring. We assessed the discrepancies in drought monitoring using remote sensing data from the Tropical Rainfall Measuring Mission (TRMM) and European Space Agency Climate Change Initiative (ESA-CCI) and European Centre for Medium-Range Weather Forecasts (ECMWF) reanalysis data (ERA5). A standardized index approach is applied to the four datasets. The indices are spatially and temporally consistent except for the ESA-CCI soil moisture (SM) dataset. The indices depict drought events over the North-West Africa region and show that the TRMM standardized precipitation index (SPI), ERA5 SPI and standardized soil moisture index (SMI) detect drought events in the Near East. A binary classification analysis showed that the indices can accurately and precisely identify drought events across the MENA region except for North East Africa. The indices show that the MENA region was recently under severe to extreme drought conditions, which are driving exploitation of available water resources in an unsustainable manner. A focus on the Haouz Plain, Morocco, and Aleppo, Syria, shows the critical situation, while the conditions over Al Jazirah, Sudan, are less critical.

Introduction

As humanity advances into the twenty-first century, the Middle East and North Africa (MENA) region is still facing the challenge of lingering droughts. The MENA region has been identified as a hot spot of climate change by the International Panel on Climate Change[1]. It is prone to extreme drought and flood events linked to climate change that are intertwined with anthropogenic activities to create a major threat[2]. The MENA region has witnessed the earliest scientific methods for water scarcity management[3]. For instance, Ancient Egypt's large dependence on Nile River flooding pushed it to invent the Nilometers: a set of installations to measure the Nile water height[4]. The Mesopotamian civilization also developed a complex system for water management to address water scarcity[5]. More recently, several studies have suggested links between natural disasters and recent conflicts in Syria[6–8], triggering massive migrations[9] and so on[10]. While a study in 2012 suggested that there has been "little change in global drought over the past 60 years"[11], several other studies have drawn another conclusion[12,13]. While outlooks into future risks have shifted to the health sector due to the coronavirus disease 201 (COVID-19) situation in 2020, in the last five years, water crises were at the top of long-term risks of the World Economic Forum (WEF) Global Risks Survey[14]. In these circumstances, the risk of water crises and food security has increased[15]. In fact, drought events account for one-fifth of the global damage caused by natural hazards[16]. Droughts have a direct impact across economic sectors, including industries and energy sectors, but the most relevant is the agronomic sector, as it accounts for 70-80% of the total volume of water use[17]. Depending on the period of vegetation growth, drought has a large impact on yield production to an extent that it poses a threat to global food security[18].

Needless to say, for the abovementioned reasons, monitoring and prediction of drought is critical. Traditionally, drought events are defined based on the geophysical variables that are analysed. The term meteorological droughts, for instance, stems from the analysis of precipitation. Agricultural droughts involve the analysis of land surface parameters, including vegetation health, soil moisture conditions, and surface temperatures. Hydrological droughts are linked to the scarcity of water resources such as snow, lakes, and groundwater, with the knowledge that 54% of irrigation is provided from surface water and 46% depends on groundwater[19]. Wilhite and Glantz[20] added a long-term dimension to drought events, with the notion of socio-economic droughts. A broader definition can also be provided when drought indices are constructed from a combination of several variables linked to the components of the earth's hydrosphere and biosphere[21].

Local approaches to drought monitoring have been continually enhanced and normalized in various stages of history

around the globe[22]. Currently, water agencies and agriculture ministries send field agents and install local sensors to create long-term databases for detecting developing droughts in a bottom-up approach. More recently, in the relative course of events, technological advancement has provided spatially distributed information through remote sensing observations and physical process modelling. This evolution started with the emergence of numerical weather prediction[23] and continued to land surface assimilation and modelling. The contribution of satellite-based Earth observation (EO) to this methodology is key. Spatial information from EO is either used to constrain the mathematical model's spatio-temporal outputs through data assimilation[24] or directly, and more in line with this research paper, by elaborating drought indices[21]. These indices can be classified based on the definition of the types of droughts mentioned earlier in this introduction. The World Meteorological Organization (WMO) in the "Lincoln Declaration on Drought Indices" issued a recommendation for the use of the Standardized Precipitation Index (SPI) as the reference index for monitoring droughts at the national level[25]. The SPI is based on the fitting of a statistical distribution to a multi-decade precipitation dataset averaged over monthly to yearly time scales and then deduces the anomaly for a given period[26].

The SPI can be obtained from EO data using Tropical Rainfall Measuring Mission (TRMM) observations[27]. Similar to precipitation, soil moisture is identified as an Essential Climate Variable (ECV)[28]. Its location at the interface between the atmosphere and the vegetation root zone makes it a highly relevant variable for water availability monitoring. The EO of soil moisture is mainly based on microwave remote sensing in the C-L bands. Multiple products have been derived from the Soil Moisture and Ocean Salinity (SMOS), Soil Moisture Active Passive (SMAP), Advanced SCATterometer (ASCAT), and Advanced Microwave Scanning Radiometer for Earth Observing System (AMSR-E) missions. Drought indices have been developed from the soil moisture and were compared to other datasets[29–32]. Vegetation health is an intermediate or late indicator of droughts depending on the selected geophysical variable. As drought develops, the water availability in the vegetation root zone decreases. Vegetation adapts to water scarcity by closing its stomata to reduce transpiration. The cooling effect of transpiration is stopped and the vegetation temperature rises. This state is called vegetation temperature stress and can be observed using the surface temperature from thermal optical EO from thermal sensors such as the one onboard the Moderate Resolution Imaging Spectroradiometer (MODIS) at a 1 km resolution[33]. In the late stages of drought, the leaves gradually dry until vegetation death. Dried vegetation can be observed using visible spectral bands. The observation of the early vegetation drying stages has been applied using the normalized difference vegetation index (NDVI) from the MODIS[34] and Advanced Very-High-Resolution Radiometer (AVHRR)[35] visible bands. A drought Vegetation Condition Index (VCI) has also been suggested[36].

From the dichotomy of drought that is presented here, precipitation and soil moisture present an advantage in terms of early warning of drought development. While they still present a drawback in terms of spatial resolution (25 to 50 km), they are hardly prone to atmospheric perturbations, as they are mostly derived from microwave data. Mixed-information drought indices have also been developed to take into consideration the coupled effect of geophysical variables[37]. For instance, the Standardized Precipitation Evaporation Index (SPEI) introduces evaporation by removing the actual evaporated water from the precipitation input, which is important for summer droughts[38]. A more complex index is the Palmer Drought Severity Index (PDSI)[39], which accounts for a two-stage bucket water budget. It has been widely used for drought assessment[40,41]. Several studies favoured the SPI and SPEI approaches over the PDSI, as it relies on the Penman-Monteith method and a large set of input datasets that propagate uncertainties in the drought index estimates[42].

This research paper addresses the intricate monitoring of drought via two remotely sensed and modelled geophysical variables, namely, precipitation and SM. The area of interest is the highly drought-prone MENA region[43]. We assess whether the differences in drought monitoring between these two pieces of information stem from the data acquisition source or from the embedded processes. We examine where and how these data can be used to efficiently monitor droughts. A four-product dataset is considered: two remote sensing and two modelling reanalysis products for each of the rainfall and soil moisture variables. The remote sensing data are obtained from the TRMM for precipitation and the European Space Agency (ESA) Climate Change Initiative (CCI) for soil moisture. The modelled datasets are obtained from the European Centre for Medium-Range Weather Forecasts (ECMWF) reanalysis data (ERA5). A standardized index approach is selected and applied to the four variables to reduce the impact of the statistical method. The demonstration starts with presenting a straightforward inter-correlation analysis of the four indices. It then expands to the detection of severe and extreme events through the four datasets at the administrative unit scale. This scale is selected due to its conformity with the water use needs of stakeholders and the resolution of the available EO data. Several regions are the focus. Based on the presented results, we provide compound answers and recommendations in the Conclusion section. The dataset description and methods are presented after the conclusion.

Results and Discussion

Consistency between the drought indices

Drought indices present the advantage of removing seasonal signals, and thus, they are readily qualified for temporal cross-correlation analysis. The consistency between the monthly precipitation and soil moisture drought indices (i.e., the SPI and soil

moisture index (SMI), respectively) using temporal cross-correlation over non-desert areas is analysed here. Figure 1 shows the six combinations of cross-correlation maps for the four datasets. The stipples plotted over the coloured map represent nodes with a significance test p-value < 0.05. The most visible result overall is that the SPI and the standardized SMI from the ERA products present the highest correlation (Fig. 1.d). This finding can be explained by the fact that the two variables are provided by the same reanalysis dataset (i.e., ERA5), and they pertain to the same assimilation system's outputs. Nevertheless, we notice that there are spots where the correlation is low, mainly in North-East Africa. This is a recurrent result across all the correlation maps. Figures 1.a-c show the correlation of the TRMM SPI with the other datasets. The TRMM and ERA5 SPIs show the highest correlation except over North-West Africa, which is consistent with previous results from[44], where monthly precipitation from the TRMM, ERA5 and ERA-Interim data were compared. Their results showed substantial improvement in the correlation of the TRMM of the ERA5 data with the ERA-Interim data over the MENA region except over North-East Africa. The result can be explained by the fact that while the processing of ERA5 does not assimilate the TRMM data, it assimilate synoptic observation (SYNOP) manual stations over the MENA region[45] that are also used in the Integrated Multi-satellitE Retrievals for Global Precipitation Measurement (IMERG) algorithm for the TRMM-ERA dataset[44], and these stations are rare over north-east Africa. The same conclusion can be drawn for the ERA SMI (Fig. 1.c). The lowest overall correlation is found when comparing the TRMM SPI to the ESA SMI (Fig. 1 b). Figures1.b,d, and f show the correlation of ESA SMI with the other datasets. The correlation shows relatively lower correlations globally with little variation across the different datasets even when the same variable, e.g., the SMI, is considered (Fig. 1.d). The coastline has a systematically lower correlation, which is mainly due to land-sea contamination impacting the soil moisture retrievals from microwave sensors at frequencies of 5-10 GHz. This is consistent with the theory of microwave remote sensing of land surfaces[46]. This phenomenon does not impact the TRMM dataset, as it is based on atmospheric observations at higher microwave frequencies of 10.7-85.5 GHz. When comparing inland areas, the cross-correlation of the ESA SMI with the ERA SPI and TRMM SPI is very close even though the ERA5 Land Data Assimilation System (LDAS) integrates the ASCAT soil moisture data[44], which is one of the ESA SMI remote sensing datasets. This finding suggests that the soil moisture-precipitation feedback into ERA5 from ASCAT is low. Another feature that can hinder the soil moisture remote sensing dataset is the presence of radio frequency interference (RFI) in Libya and South Sudan, which mainly impacts passive microwave remote sensing technologies (AMSR-E, AMSR-2)[47]. In summary, the ERA SMI and SPI and the TRMM SPI show more consistent results than the ESA SMI. Low correlation is observed over North-East Africa, and the highest correlation is observed in North-West African (Maghreb).

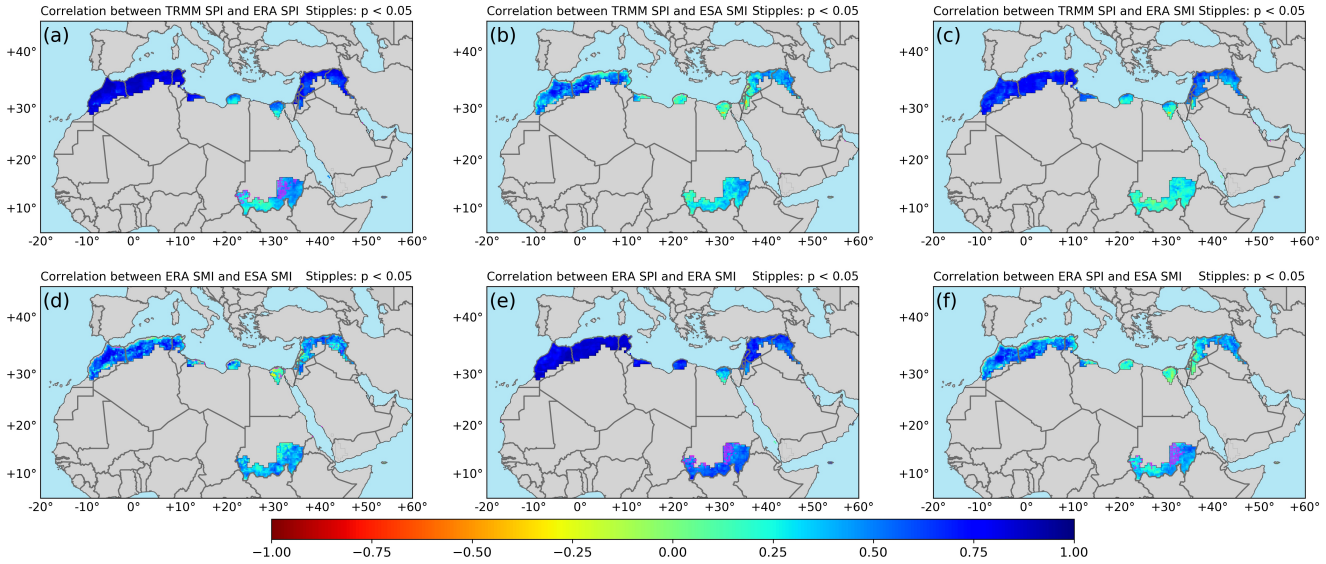

Figure 1. Pearson temporal cross-correlation maps for the four considered drought indices: Corr(TRMM SPI, ERA SPI) (a), Corr(TRMM SPI, ESA SMI) (b), Corr(TRMM SPI, ERA SMI) (c), Corr(ERA SPI, ESA SMI) (d), Corr(ERA SPI, ERA SMI) (e), and Corr(ERA SPI, ESA SMI) (f).

Detection capacity of the drought indices

The validation of a drought index is a complex exercise due to its probabilistic nature. Often, the validation exercise consists of directly evaluating the performances of the input geophysical variables or indirectly via the drought impacts[43]. For the objective of providing a validation exercise, the drought indices are compared using binary classification to a drought observation

database that was constructed in this study based on an extensive set of reports, news outlets, and scientific articles [The MENA Region and Drought database]. Figure 2 shows the true positive rate (TPR) (equation 5) and the false positive rate (FPR) (equation 6) for the four datasets over the MENA region at the country scale while excluding desert areas, considering the months from November to April over the period 1998 to 2017 and a standardized value for the drought index $\leq$-1.5. The choice of the drought index threshold is guided by the fact that the registered drought events in the validation database correspond to severe and extreme conditions. The TPR, which corresponds to the hit rate, reaches values higher than 0.9 over several countries in MENA for all indices except for the ESA SMI, which reaches a maximum TPR of 0.8-0.9 over North-West Africa (Maghreb). The FPR, which corresponds to the missed rate, is lower than 0.4 overall with the best performance over North-West Africa (Maghreb) (FPR < 0.2) for all the indices except the ERA SMI. When analysing the results in terms of geophysical variables, the precipitation-based drought indices from the TRMM and ERA5 show a higher TPR than the soil moisture-based indices from ESA-CCI SM and ERA5 data. When considering the results in terms of geography, the Middle East shows the highest spatial variability of TPR and FPR across the drought indices. The best performances for the Yemen region were found for the ERA SPI (TPRs of 0.8-0.9 and FPRs of 0.3-0.4). To better show the distribution across geographic regions, the FPR

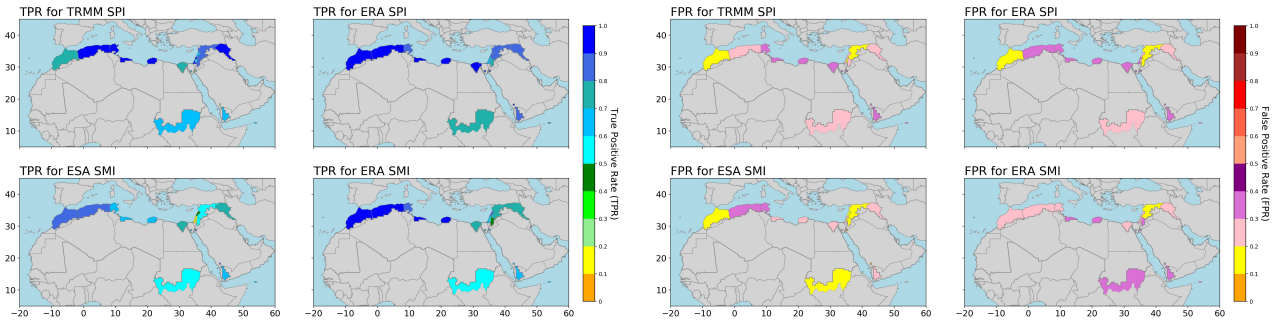

Figure 2. True positive rate (TPR) (left) and false positive rate (FPR) (right) for the TRMM SPI, ERA SPI, ESA SMI, and ERA SMI drought indices against the constructed drought database.

and TPR were aggregated over North-West Africa (Maghreb), North-East Africa (Nile basin), and the Middle East in Table 1. North-East Africa (Nile basin) shows the lowest TPR and the highest FPR for the TRMM and ERA datasets. This result is consistent with global precipitation comparison exercises[48] and validation exercises focusing on this region[49]. The ESA SMI under-performs over the Middle East (TPR = 0.42). This finding is expected because the dataset contains long gaps and is inconsistent with all other datasets, as shown in the correlation analysis. The best overall performances are obtained over North-West Africa (Maghreb) (TPR > 0.9 for the TRMM and ERA5 indices). The SMI from ESA and ERA showed good overall detection ratios over North-West Africa, which is consistent with previous studies showing the utility of soil moisture data for drought monitoring in this region[30]. The FPR for the selected regions varies between 0.16 and 0.31. While the ESA SMI achieves the lowest FPR, it also presents the lowest TPR, which implies that the total number of detected (true and false) events is low compared with that of the other datasets. The low performances of the ESA-CCI SM data for detecting droughts in arid to semi-arid regions have already been pointed out[50].

Index / Region	TRMM SPI		ESA SMI		ERA SPI		ERA SMI	
	TPR	FPR	TPR	FPR	TPR	FPR	TPR	FPR
North-West Africa: Maghreb	0.90	0.30	0.71	0.26	0.94	0.29	0.92	0.31
North-East Africa: Nile basin	0.71	0.28	0.63	0.21	0.87	0.32	0.63	0.20
Middle East	0.79	0.18	0.42	0.16	0.76	0.23	0.65	0.24

Table 1. True positive rates (TPRs) and false positive rates (FPRs) over the North-West Africa, North-East Africa, and Middle East MENA regions.

To determine the drought event detection accuracy and precision with respect to the selected drought index threshold, the detection was re-run using varying thresholds for each of the indices. The resulting accuracy (equations 7 and precision (equation8) for the MENA region and the three aforementioned regions of interest are plotted in Figures 3.a and b. The accuracy and precision over North-East Africa (Nile basin) achieve the lowest relative performances, except for the ESA SMI. The reason that the ESA SMI achieved higher precision while providing a lower hit rate and a higher missed rate is the very low number of detected events in the region of interest, which artificially increased the precision. Over all, the accuracy ranges between 0.65 and 0.82 with wide variability across the regions and datasets. The accuracy is on average lower at the edges (-2 and

-1). At $threshold = -2$, the number of events is low, which explains the reduced detection performance. A $threshold = -1$ corresponds to nominal conditions. Interestingly, the highest accuracy is reached at approximately $threshold = -1.5$, which is the recommended value for severe droughts[51]. The precision increases as the threshold decreases, which corresponds to more severe droughts and can be explained by the reduced number of drought events. This implies that a dataset with a longer time series is needed for determining the detection precision. The accuracy for the SMIs is lower than the equivalent values for the SPIs independent of the data source (i.e., remote sensing or reanalysis data). This finding can be associated with the more heterogeneous nature of the SM data, which encodes precipitation and evapo-transpiration dynamics.

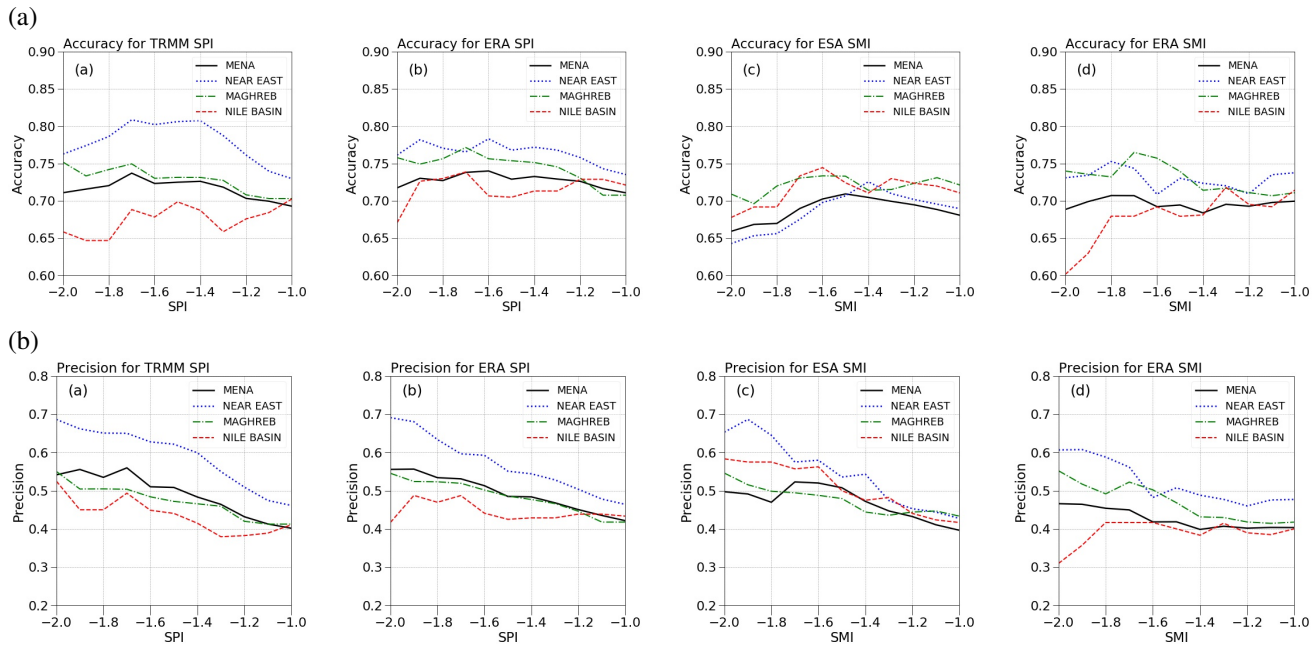

Figure 3. Accuracy and precision of the TRMM SPI, ESA SMI, ERA SPI, and ERA SMI with respect to the constructed drought dataset.

State of droughts in the MENA region over the last two decades

The last two decades were particularly dry over the Mediterranean region compared to the last 65 years[52] and even last centuries[53]. How droughts are spatially and temporally distributed across the MENA region is shown here with no aim at determining the drought frequency or return period, as it requires a very long time series, which are not available from remote sensing datasets. The drought index was determined over each administrative level-1 area (governorates, provinces, wilayas, muhafazat) based on the median value and the total number of months with severe to extreme droughts from November through April of each year (Fig. 4). The maps show a large number of regions with more than 24 months of droughts over the last twenty years. The regions with the highest number of drought months are North-West Africa and North-East Africa. The precipitation indices (TRMM SPI and ERA SPI) show a higher number of drought months, which can be attributed to the more statistically stationary nature of precipitation with respect to soil moisture. In an effort to investigate a direct application of the drought indices, no normalization was performed with the total number of available months. Thus, the gaps in the ESA SMI directly penalize the number of depicted drought months. The total number of dry months in North Africa and the Middle East can be linked to the vegetation cover. Vegetated regions are more prone to drought, while dry to desert areas are less prone to drought[30]. This impact is even more visible using the SMIs than the SPIs.

The most severe drought events are distributed across years and regions. While the droughts in Syria were very extreme for 2008-2013, several indices show even a more critical situation for more recent drought events from 2013-2018 (Fig. 5). The 5-year class of the worst droughts in North-West Africa is even more distributed across the indices. For Algeria and northern Morocco, 1998-2008 appears to be the decade with the worst droughts. For southern Morocco, the 2008-2018 decade is more prominent in terms of extreme drought events. The worst droughts in North-East Africa are identified for the 2008-2018 decade across all the indices. A focus on the Morocco, Syria and Sudan situations with a wider view that includes groundwater, rivers, and lake water resources is provided in the next section.

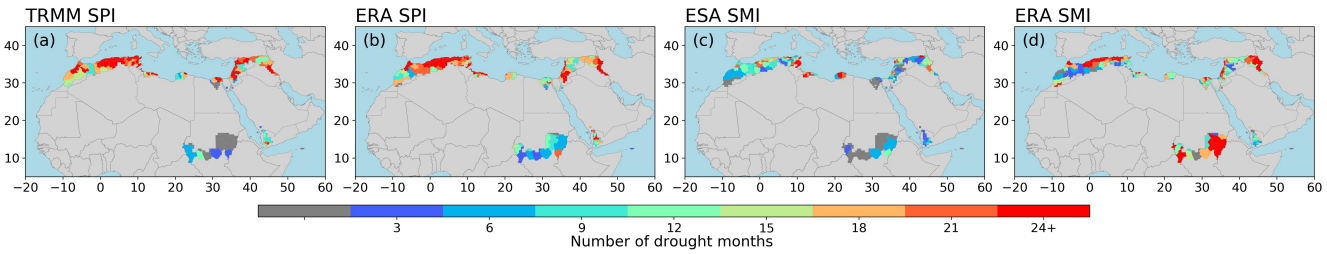

Figure 4. Number of months with severe to extreme drought events (index < -1.5) from 1998-2018 at administrative level 1 across the MENA region, from the TRMM SPI (a), ERA SPI (b), ESA SMI (c), and ERA SMI (d).

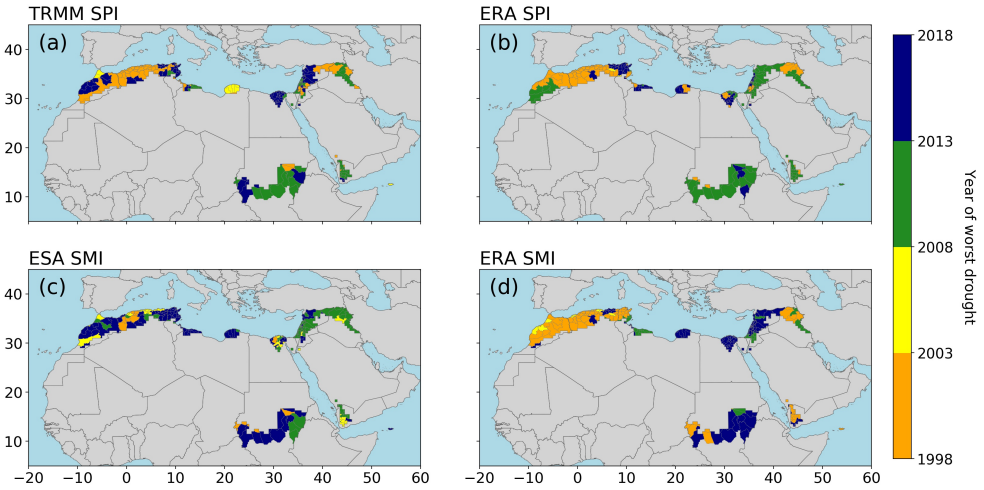

Figure 5. Period of most extreme drought by class for the 5 years from 1998-2018 for the TRMM SPI, ERA SPI, ESA SMI and ERA SMI for each column.

Drought events, irrigation, and water resources across the MENA region

As drought develops, more stress is applied to the available water resources. In many cases, in the MENA region, these resources are exploited at an unsustainable level. Therefore, when analysing drought events, it is important to consider the available water resources at the regional scale. These stocks are either in the form of surface water (rivers, lakes) or groundwater. We present to the reader three case studies with analysis of drought events (Fig. 6) in link to the existing water resources (Fig. 7). Notably, the river, dam and lake heights were obtained from remote sensing altimetry. The aim of the results is to show the use of drought indices in contextualized conditions and to assess the relevance of the very recent droughts depicted in the previous section.

Haouz Plain, Morocco

The Haouz Plain is an agricultural area located within the Tensift watershed in southern Morocco near the city of Marrakech. The climate is arid to semi-arid, with an average yearly rainfall of 250 mm/year. Irrigation is intensely and extensively applied. It is provided from surface water and groundwater. Surface water irrigation depends on supplies from the Lalla Takerkoust, Moulay Youssef, and Hassan 1 reservoirs through irrigation canals[58]. An estimated 25% of the streamflow is generated by snow melt[59]. The time series of drought indices with associated histograms over the Haouz Plain are shown in Figure 6.a. The TRMM-ERA SPI time series shows very good consistency, while the ESA-ERA data are more consistent after 2005, which coincides with the addition of satellite sensors more adapted for soil moisture observations [Remote sensing soil moisture dataset]. Abrupt changes due to the choice of sensors are detectable. The well-documented extreme droughts of 2001 and 2016 can be easily depicted by the indices. Severe drought events are frequent with a strong developing drought in the last three years of the dataset. The decadal analysis of the drought indices in the histograms shows an increase in drought events (Fig. 6.a). When comparing the statistical distribution of irrigated areas versus the surrounding closest non-irrigated areas in terms of precipitation (Fig. 8.a) and soil moisture (Fig. 8.b), the impact of irrigation can clearly be identified. The statistical distribution of precipitation is very similar between agricultural and non-agricultural areas ($\Delta median = 5mm/month$). The soil moisture dataset shows a relatively strong discrepancy between the two areas, with agricultural areas much wetter

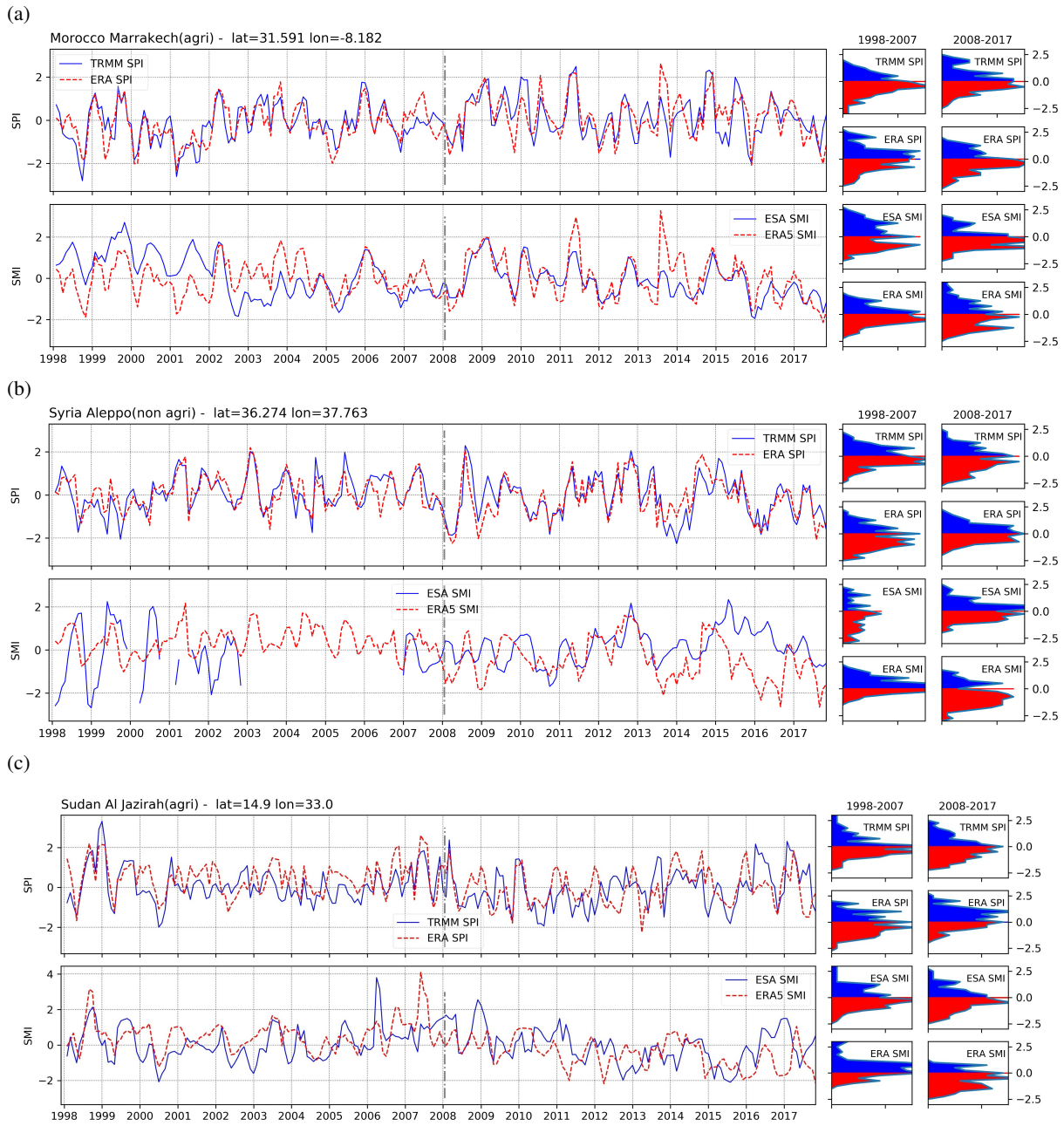

Figure 6. Time series (left) and histogram (right) of the SPI and SMI for Marrakech in Morocco, Aleppo in Syria, and Al Jazirah in Sudan. The histograms are divided into two decades for each of the four datasets.

($\Delta median = 0.06 m^3/m^3$). The persistence of wetter conditions is ensured by irrigation in this arid to semi-arid region.

When the groundwater levels are considered, the situation can be better comprehended, as shown in Figure 7.a. The groundwater resources are exploited at a unsustainable rate, inducing a decrease in the groundwater level at approximately 1-3 m/year[55,60]. The Moroccan government triggered conversion to drip irrigation through financial incentives that fostered intensification and conversion to cash crops (tree crops), threatening even more groundwater resources. The combined interlinked effect of irrigation and drought diminishes water resources in an unsustainable manner. The very recent droughts will pose a great challenge.

Aleppo plateau, Syria

Food security is a major concern in Syria since the rise of the Syrian conflict in 2011, which has impacted more than 2.5 million residents[61]. The Syrian conflict coincided with the end of a long period of drought and caused the displacement of 6.2 million

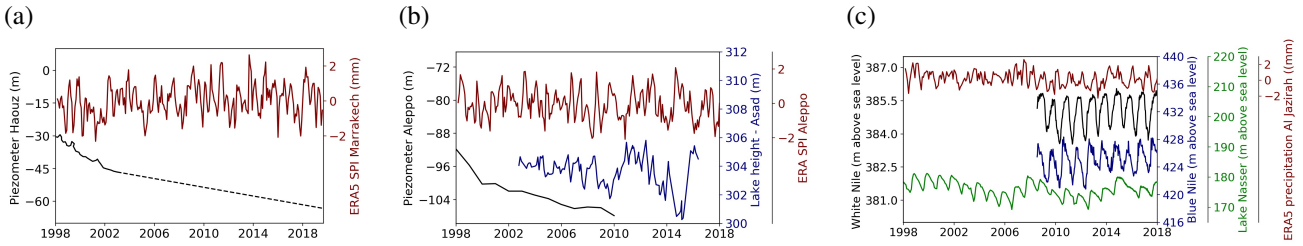

Figure 7. Time series of soil moisture from the ERA SPI and water levels of rivers, lakes and groundwater. (a) Haouz Plain, Morocco: groundwater level from[54] until 2002 (Hydraulic Agency) and extrapolated to 2019 by considering a constant rate of 1 m/year based on[55], (b) Aleppo, Syria: groundwater level from[56,57], and (c) Al Jazirah: White Nile, Blue Nile and Lake Nasser levels.

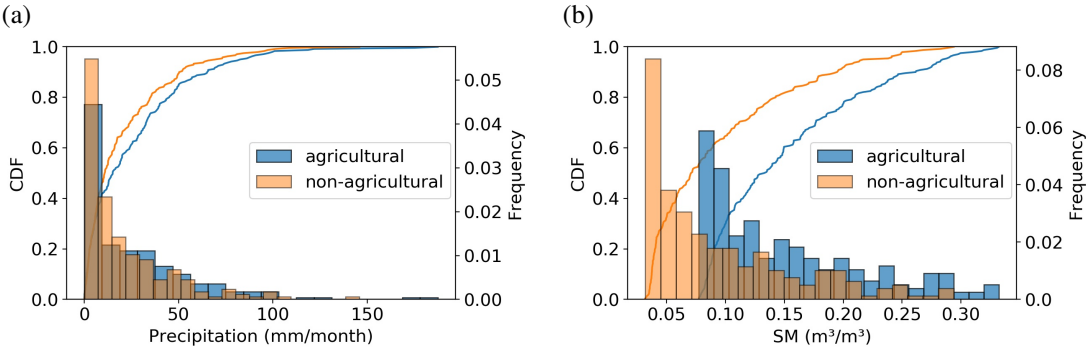

Figure 8. Statistical distribution of precipitation and soil moisture from ERA5 over agricultural and adjacent non-agricultural nodes in the Haouz Plain, Morocco.

Syrians. The Aleppo region is an essential agricultural area in Syria. The crops in the region were traditionally wheat and cotton during the winter season with additional irrigation and have diversified to wheat, cotton, tobacco, sugar beet, barley, lentils, chickpeas, fruits and vegetables during the last two decades. The major droughts of 2008 and 2016[53] are depicted by the four datasets (Fig. 6.b). The time series also shows that the precipitation drought index variations are consistent, while the soil moisture indices show many disagreements. The histograms show a more contrasting climate with strong extremes of wet and very dry conditions, as projected by the International Panel on Climate Change (IPCC)[1]. The predominant dry conditions from 2008 to 2017 are best depicted in the ERA SMI dataset. The dataset also shows very dry conditions in recent years. Agriculture in Aleppo relies highly on irrigation. Irrigation water is provided by channel irrigation from the Euphrates and groundwater pumping. During the last decade, the irrigation amounts for cotton and wheat were higher than the technically recommended levels and reached unsustainable levels[57]. The levels in the artificial Lake Assad on the Euphrates have shown a continuous drop since 2002 with a strong increase in 2016 (Fig. 7.b). On the other hand, the ground water levels have continually decreased since the 1980s (at approximately 1.5 m/year) and have reached dry conditions in several wells[56,57] (Fig. 7.b).

Al Jazirah, Sudan

Wilayat Al Jazirah, Sudan, is located between the Blue Nile in the north-west and the White Nile in the west. It is a major agricultural area in Sudan with more than 10,000 km^2 of irrigated fields, making it one of the largest irrigation projects in the world. The crops are mainly cotton along with several varieties of cash crops (millet, pulses, wheat). Rainfall occurs mainly during July and August and is extremely scarce during the winter months. Irrigation is practised during the winter season for cotton. The major drought events over Al Jazirah during 2008 and 2016 are depicted by the four datasets (Fig. 6.c). The ESA SMI shows abrupt changes at the other sites due to the heterogeneity among the applied sensors. Most interestingly, the four datasets show a strong aggravation of the SPIs and SMIs during the last five years with several extreme drought events. This finding is also clear in the histogram of the drought indices, which show a higher probability of dry conditions during the 2008-2018 decade than for the the 1998-2007 decade. Considering the importance of this region to the entire economy of Sudan, these conditions can have direct socio-economic consequences. It is also vital information since the regional strategic water management scheme has shifted since the 1980s from foreign exchange earnings to sustain food security[62]. In the long term, the IPCC projections show, on average, an increase in rainfall of approximately 40 mm for the period from 2040 to

2070 combined with increased evapo-transpiration due to increased temperatures, but this phenomenon is combined with more extreme droughts and floods[1]. The situation may be further exacerbated as the dependence on irrigation will increase while the potential Grand Ethiopia Renaissance Dam (GERD) being constructed upstream of the Blue Nile[63]. Currently, the levels of the Blue Nile, White Nile and Lake Nasser downstream of the Nile River show an increase in water levels (Fig. 7.c), which should enable compensation with proper water management of recent drought conditions.

Criticality of drought events over the MENA region

By 2025, 1.8 billion people will experience absolute water scarcity, and two-thirds of the world will be living under water-stressed conditions[64]. The MENA region, with an area of approximately 10 million km^2, has a prevailing hot and dry climate with only some areas that have sub-humid and humid climates. The worldwide average water availability is approximately 7000 $m^3/cap/year$, while in the MENA region, it reaches 1200 $m^3/cap/year$[65]. Drought monitoring is crucial for countries in the MENA region. We showed that the SPI and SMI drought indices are spatially and temporally consistent to a lesser extent for the ESA-CCI SM data. Our results suggest that for multi-decade applications of the ERA-CCI SM dataset, efforts should be invested to better homogenize and gap-fill the time series. The comparison to the drought database assembled in this paper delivers insights into the capacity of the precipitation- and soil moisture-based drought indices to detect drought across the MENA region. The spatial patterns in the true detection results matched the expected ones, with several areas showing a perfect hit score (1.0). An assessment of the droughts over the MENA region in the last two decades shows the severity of recent droughts. We did not assess the impact of climate regimes such as the North Atlantic Oscillation (NAO) on these results, as 20 years is a short period, but it is clear from the detected cases that the MENA region is still experiencing extreme droughts. However, to properly interpret the drought index results, it is important to consider the available water resources for irrigation. The analysis in the cases of the Haouz Plain, Morocco, and Aleppo, Syria, shows the high stress on the water resources when considering groundwater and drought events. The situation in Al Jazirah, Sudan, is less alarming when considering the water levels of the White Nile, Blue Nile and Lake Nasser, even though recent drought conditions are apparent. In summary, desertification and reduction of agricultural areas are highly probable over many regions in the MENA region, which could develop into a food security crisis.

Data and Methods

The MENA region and the associated drought database

The MENA region has no strict political or organisational definition. In this paper, we refer to the reduced extents of the MENA region, which is mainly defined by the southern part of the Mediterranean Sea from Syria to Morocco and the Arabic Peninsula. It can be divided into the Maghreb region, the North-East Africa region, and the Middle East (or West Asia) region. The MENA region, with an area of approximately 10 million km2, has a prevailing hot and dry climate with only some areas that have sub-humid and humid climates. The MENA region as defined here has a population of approximately 374.9 million people[66]. The region has climate impacts from the Mediterranean Sea, the surrounding deserts and the NAO[67,68]. It is also identified as a hot spot of climate change by the IPCC[1]. The North-West African (Maghreb) region is bounded by deserts in the south and the Mediterranean Sea to the north. The agricultural landscape in this area is mainly composed of field crops and olive trees. The field crops are mainly wheat, barley and oat, which make up approximately 46% percent of the cultivated area. Olive orchards represent approximately 14% of the agricultural area but are very dominant in Tunisia, with 2 million hectares[30]. The North-East African part of the MENA agricultural areas is dominated by the Nile River basin, which concentrates along its path along the agricultural areas. The Middle East region consists of semi-arid to desert areas and has witnessed numerous drought events in the last two decades. Administrative division level 1 (provinces, governorates, wilayas, muhafazat) was selected for the drought analysis since the mitigation and adaptation measures concerning droughts are applied at this scale based on the Global ADMinistrative Areas Database (GADM)[69]. Since drought is a major threat in the MENA region, it is monitored closely by administrations, international organisations, and the scientific community. Therefore, there is a plethora of resources on drought in the form of reports, scientific papers, and media outlets. While a global database with regional-scale aggregation of drought events exists, it does not present separate events across the MENA region[52]. In this paper, a "drought history database" was assembled from a collection of sources on the occurrence of drought in the Middle East and North Africa spanning the same period as the remote sensing and modelling datasets, namely, from 1998 to 2017. This database consists of the reference database for the verification of drought detection from standardized indices across the MENA region. The density of information differs across the region's countries. Those with more agricultural production (the Maghreb region, Egypt and east of the Mediterranean) have more articles and reports on droughts as they are dependent on sufficient water resources during their growing seasons. In contrast, countries with largely dominant desert and arid areas, such as the KSA and UAE, are less studied, and few localized studies on drought and drought impacts have been identified over these areas. Table (2) summarises

the findings at the country level. It was constituted based on three sources: international and local organisations[70–73], scientific papers[74,74–81], and media and database portals[61,82–86].

Country	Year	Country	Year	Country	Year	Country	Year	Country	Year
Lebanon	1999	Morocco	1999	Tunisia	1999	Syria	1999	Algeria	1999
	2000		2000		2000		2000		2000
	2001		2001		2001		2001		2001
	2003		2002		2002		2006		2002
	2008		2005		2008		2007		2004
	2010		2006		2010		2008		2007
	2012		2008		2013		2009		2008
	2013		2012		2015		2010		2009
	2014		2015	Sudan	1998		2013		2015
	2016		2016		2000		2014		2016
Jordan	1999	Yemen	1998		2002		2015	Bahrain	2000
	2000		1999		2003		2016		2001
	2004		2008		2005	UAE	1999		2009
	2006		2009		2006		2000		2012
	2007		2018		2007		2002		
	2008	Qatar	2000		2008		2004		
	2009		2001		2009		2007		
	2013		2009		2010		2010		
	2014		2012		2011		2012		
	2015	Iraq	1999		2017		2016		
KSA	1998		2000	Oman	1999	Mauritania	1999		
	1999		2006		2002		2004		
	2009		2007		2004		2011		
	2012		2008		2006		2012		
	2017		2009		2007		2013		
Kuwait	2001		2010		2011		2014		
	2007		2011		2013	Israel/Palestine	1999		
	2008		2012	Libya	1999		2000		
	2009	Egypt	1999		2008		2001		
	2010		2002		2010		2007		
	2012		2009		2015		2008		
	2015		2010		2016		2014		

Table 2. Drought years in the MENA region from 1998 to 2017 based on the literature.

Remote sensing and reanalysis datasets

Drought is assessed through two geophysical variables: cumulative rainfall (mm) and soil moisture averages (m^3/m^3). Precipitation is commonly used for meteorological drought monitoring at 1-month averages and agricultural drought monitoring at 1-6-month averages. The monthly average soil moisture has the advantage of combining the impact of rainfall and soil evaporation. For each geophysical variable, a remote sensing and a reanalysis dataset are considered to identify the differences that arise from the data source or physical processes. The details of the analysed datasets are presented in Table (3). A standardized drought index is derived for each dataset.

Drought index	Product name	Type	Source	Spatial resolution	Reference
TRMM-SPI	TRMM-3B43v7	remote sensing	TRMM mission	$0.25° \times 0.25°$	Huffman et al. 2007[87]
ESA-SMI	ESA-CCI-SMv2.0	remote sensing	multi-mission	$0.25° \times 0.25°$	Dorigo et al. 2017[88]
ERA-SPI	ERA5	reanalysis	IFS (CY41R2)	$0.25° \times 0.25°$	Dee et al. 2011[44]
ERA-SMI	ERA5	reanalysis	IFS (CY41R2)	$0.25° \times 0.25°$	Dee et al. 2011[44]

Table 3. Datasets used to compute the drought indices.

Remote sensing precipitation dataset

The TRMM-3B43 (version 7) product was used in this study[27]. It consists of monthly averages of TRMM-3B42 (in mm/h) with a spatial resolution of $0.25^\circ \times 0.25^\circ$. The TRMM-3B42 product combines remotely sensed precipitation estimates corrected with land surface gauge analyses. The monthly average precipitation was extracted over the region of interest for the period extending from 1998 to 2018. TRMM-3B43 is based on data from the TRMM and the Global Precipitation Mission (GPM) using the IMERG algorithm. The TRMM is a joint EO satellite mission between the NASA and the Japan Aerospace Exploration Agency (JAXA), previously the Japanese National Space Development Agency (NASDA), with the objective of measuring tropical and subtropical precipitation[87]. The TRMM ended in 2015, and the GPM is the successor mission.

Remote sensing soil moisture dataset

The ESA-CCI provides long-term consistent archives of data for several ECVs, aiming at enhancing the knowledge on the effects of climate change. The ESA-CCI SM dataset addresses the surface soil moisture ECV. It is available globally at daily time steps from 1978 onward and over a $0.25^\circ \times 0.25^\circ$ grid. The initiative produces a consistent remotely sensed soil moisture dataset from the observations of a multitude of active/massive microwave sensors (Special Sensor Microwave Imager (SSM/I), ASCAT, AMSR-E, SMOS, SMAP, and AMSR-2) at different spectral bands (X, C, K, and L)[88]. The choice of sensors changes over time and in space depending on the available platforms to take advantage of the advantages of the most adequate sensor technology at each location. In the case of the MENA region, the data are predominantly provided by the SSM/I sensors from 1998 to 2002, the AMSR-E sensor from 2002 to 2007, and the AMSR-E and ASCAT sensors after 2007. The daily ESA-CCI data were downloaded and extracted over the area of interest. The monthly cumulative precipitation and average soil moisture were then computed.

Precipitation and soil moisture reanalysis data

Reanalysis in weather forecasting consists of re-running the integrated forecast and assimilation system to produce consistent global datasets. Reanalysis is essential for climate change studies and extreme event monitoring. Here, the ERA5 dataset was used. ERA5 is the latest global reanalysis dataset produced by the ECMWF. ERA5 is produced using 4D-Var data assimilation in CY41R2 of ECMWF's Integrated Forecast System (IFS), with 137 hybrid sigma/pressure (model) levels in the vertical direction, with the top level at 0.01 hPa[44]. The land model in ERA5 is the Hydrology Tiled ECMWF Scheme for Surface Exchanges over Land (HTESSEL). ERA5 replaces the ERA-Interim data[89] and improves upon it across various aspects. One of the major improvements in ERA5 is the much higher spatial and temporal resolution, better global balance of precipitation and evaporation, and better soil moisture estimates[90]. The ERA5 data cover the period from 1950 up to 2 months before the present month at a $0.25^\circ \times 0.25^\circ$ spatial resolution and various time steps. Monthly cumulative precipitation and monthly average surface soil moisture (layer 1) data from 1998 to 2017 from the ERA5 dataset were used.

Rivers and lake water heights from remote sensing altimetry

The water levels (in metres) for the virtual stations were acquired from the Hydroweb database[91]. The water levels are retrieved by radar altimetry satellites over virtual stations in rivers[92] and lakes[93]. The time series data are constructed from the acquisitions of the Joint Altimetry Satellite Oceanography Network (Jason), Jason-2, Jason-3, and Sentinel-3 satellites. The Jason series operates at Ku-band (13.575 GHz) and C-band (5.3 GHz). Jason-2 was launched in 2008 and ended operations in 2019. Jason-3 was launched in January 2016. The Sentinel-3A altimetry satellite operates at Ku-band (13.575 GHz) and C-band (5.41 GHz) and was launched in February 2016. Table 4 shows the details of the used virtual stations.

Case	Type	Name	Lat	Long	Start date	End date
Aleppo, Syria	Lake	Assad	36.0	38.17	10/10/2002	22/05/2016
Al Jazirah, Sudan	Lake	Nasser	22.8	32.57	27/09/1992	28/09/2020
Al Jazirah, Sudan	River	Blue Nile	13.2598	33.9004	17/07/2008	22/09/2020
Al Jazirah, Sudan	River	White Nile	22.8	32.57	19/07/2008	25/09/2020

Table 4. Altimetric river and lakes heights.

SPI and SMI

The SPI is widely used for assessing droughts[26,42,94,95]. It is obtained by fitting a given probability density function to a long historical record of cumulative rainfall data and then by deducing the percent point function (ppf). The main advantage of this approach is that it provides relevant information across locations and can be used for a variety of timescales. The approach was also applied to the soil moisture data; in this case, the index is identified as the SMI. Time series of cumulative and averaged data over each node of the precipitation and soil moisture datasets were generated using 3-month periods. In this paper, we refer indifferently to SPI-3 as the SPI. The Weibull distribution and the more commonly used gamma distribution were tested,

and the gamma distribution was finally selected to fit the data. The gamma distribution probability density function for variable X with a time constant (t) is given in its integral form by equation (1).

$$f(x) = \beta^{\alpha} x^{\alpha-1} e^{-\beta x} \Gamma(\alpha)^{-1} \tag{1}$$

where x is a random variable, α is the shape parameter, and β is a rate parameter with $\alpha,\beta > 0$. $\Gamma(\alpha)$ is the gamma function given equation(2).

$$\Gamma(\alpha) = \int_0^{\infty} x^{\alpha-1} e^{-x}\, dx,\ \alpha > 0. \tag{2}$$

The gamma distribution was fit to each pack of data records across the time series (i.e., the month of the year for the monthly data) using an optimization scheme based on maximum likelihood estimation. The extracted set of values (i.e., 12 for the monthly data) of α and β were then used to generate the ppf, which also corresponds to the cumulative distribution function. These correspond to the SPI values, which are then used to discriminate dry and wet conditions. The qualifications of the wet and dry conditions with respect to the SPI values are presented in Table (5) based on[51].

Standardized index value	Conditions
2+	extremely wet
1.5 to 1.99	very wet
1.0 to 1.49	moderately wet
-.99 to .99	near normal
-1.0 to -1.49	moderately dry
-1.5 to -1.99	severely dry
-2 and less	extremely dry

Table 5. Drought conditions with respect to the SPI values, adapted from[51]

Temporal cross-correlation for consistency analysis

Pearson's correlation is computed based on the time series at each node for each pair of datasets (equation (3)).

$$R = \frac{cov_{x,y}}{\sigma_x \sigma_y} \tag{3}$$

where σ_x and σ_y are the variances of the time series for variables x and y, respectively, and cov is the covariance of x and y (4).

$$cov_{x,y} = \frac{\sum_{i=1}^{N}(x_i - \bar{x})(y_i - \bar{y})}{N-1} \tag{4}$$

where N is the total number of time records from x and y.

The significance test using the p-value, which is the probability that the null hypothesis is true, was added to the correlation maps. The null hypothesis corresponds to the case where two measured phenomena are not related to each other. A $p-value \leq 0.05$ was considered statistically significant.

Binary classification for drought index evaluation

Drought detection via the four standardized indices were compared to the historical drought dataset using binary classification. The historical dataset is applied at administrative division level 1 (governorates). Droughts from November to April were considered. The TPR and the FPR were computed using equations (5 and 6), respectively. The TPR is the successful drought detection rate. The FPR corresponds to the false drought alert rate. The accuracy and precision are computed using equations (7 and 8), respectively. The accuracy is representative of the ability of the drought index to detect drought and non-drought conditions, while the precision assesses the dispersion of the predictions.

$$TPR = \frac{\sum(TP)}{\sum(TP+FN)} \tag{5}$$

$$FPR = \frac{\sum(FP)}{\sum(FP+TN)} \tag{6}$$

$$Accuracy = \frac{\sum(TP+TN)}{\sum(TP+TN+FP+FN)} \tag{7}$$

$$Precision = \frac{\sum(TP)}{\sum(TP+FP)} \tag{8}$$

where TP is the number of true positives, TN is the number of true negatives, FP is the number of false positives, and FN is the number of false negatives.

Data Availability

All data used in this study are publicly available with an open licence for non-commercial use. They were all last accessed on 10/10/2020.

- The TRMM 3B43 dataset is available at https://disc.gsfc.nasa.gov/datasets/TRMM_3B43_7
- The ESA-CCI SM dataset is available at https://www.esa-soilmoisture-cci.org/
- The ECMWF ERA5 dataset is available at https://www.ecmwf.int/en/forecasts/datasets/
- Administrative division maps are available at http://www.gadm.org
- Water level heights and lake heights from altimetry are available at http://hydroweb.theia-land.fr/

References

1. Seneviratne, S. *et al.* Changes in climate extremes and their impacts on the natural physical environment in: Managing the risks of extreme events and disasters to advance climate change adaptation. *A Special Rep. Work. Groups I II Intergov. Panel on Clim. Chang. (IPCC)* 109–230 (2012).
2. Sowers, J., Vengosh, A. & Weinthal, E. Climate change, water resources, and the politics of adaptation in the middle east and north africa. *Clim. Chang.* **104**, 599–627 (2011).
3. Viollet, P.-L. *Water Engineering in Ancient Civilizations: 5,000 Years of History* (CRC Press, 2017).
4. Ardagh, J. Nilometers. In *Proceedings of the Royal Geographical Society and Monthly Record of Geography*, vol. 11, 28–38 (JSTOR, 1889).
5. Tamburrino, A. Water technology in ancient mesopotamia. In *Ancient Water Technologies*, 29–51 (Springer, 2010).
6. Kelley, C. P., Mohtadi, S., Cane, M. A., Seager, R. & Kushnir, Y. Climate change in the fertile crescent and implications of the recent syrian drought. *Proc. national Acad. Sci.* **112**, 3241–3246 (2015).
7. Ide, T. Climate war in the middle east? drought, the syrian civil war and the state of climate-conflict research. *Curr. climate change reports* **4**, 347–354 (2018).
8. Gleick, P. H. Water, drought, climate change, and conflict in syria. *Weather. Clim. Soc.* **6**, 331–340 (2014).
9. Dworak-Peck, S. Fleeing drought: The great migration to europe. In Palinkas, L. A. (ed.) *Global Climate Change, Population Displacement, and Public Health*, 71–98 (Springer, 2020).
10. Sternberg, T. Regional drought has a global impact. *Nature* **472**, 169–169, DOI: 10.1038/472169d (2011).
11. Sheffield, J., Wood, E. F. & Roderick, M. L. Little change in global drought over the past 60 years. *Nature* **491**, 435–438 (2012).
12. Dai, A. Increasing drought under global warming in observations and models. *Nat. climate change* **3**, 52–58 (2013).
13. Briffa, K., Van Der Schrier, G. & Jones, P. Wet and dry summers in europe since 1750: evidence of increasing drought. *Int. J. Climatol. A J. Royal Meteorol. Soc.* **29**, 1894–1905 (2009).

14. World Economic Forum. The global risks report 2019. http://www3.weforum.org/docs/WEF_Global_Risks_Report_2019.pdf (2019). Accessed: 2020-10-10.

15. Food Security information Network. Global report on food crises 2020. https://www.wfp.org/publications/2020-global-report-food-crises (2020). Accessed: 2020-10-10.

16. Wilhite, D. Drought: A global assessment. *Nat. Hazards Disasters Ser.* **1** (2000).

17. Cosgrove, C. E. & Cosgrove, W. J. *The United Nations World Water Development Report Nb 4: The Dynamics of Global Water Futures: Driving Forces 2011–2050*, vol. 2 (UNESCO, 2012).

18. Schmidhuber, J. & Tubiello, F. N. Global food security under climate change. *Proc. Natl. Acad. Sci.* **104**, 19703–19708 (2007).

19. Siebert, S. *et al.* Groundwater use for irrigation—a global inventory. *Hydrol. earth system sciences* **14**, 1863–1880 (2010).

20. Wilhite, D. A. & Glantz, M. H. Understanding: the drought phenomenon: the role of definitions. *Water international* **10**, 111–120 (1985).

21. Zargar, A., Sadiq, R., Naser, B. & Khan, F. I. A review of drought indices. *Environ. Rev.* **19**, 333–349 (2011).

22. Howe, G. M. Agro-climatic analogues. *Nature* **161**, 983–984 (1948).

23. Shuman, F. G. History of Numerical Weather Prediction at the National Meteorological Center. *Weather. Forecast.* **4**, 286–296, DOI: 10.1175/1520-0434(1989)004 (1989). https://journals.ametsoc.org/waf/article-pdf/4/3/286/4649218/1520-0434(1989)004_0286_honwpa_2_0_co_2.pdf.

24. Zhang, Z. & Moore, J. C. Chapter 9 - data assimilation. In Zhang, Z. & Moore, J. C. (eds.) *Mathematical and Physical Fundamentals of Climate Change*, 291 – 311, DOI: https://doi.org/10.1016/B978-0-12-800066-3.00009-7 (Elsevier, Boston, 2015).

25. Hayes, M., Svoboda, M., LeComte, D., Redmond, K. & Pasteris, P. The lincoln declaration on drought indices. *Bull. Amer. Meteor. Soc* **92**, 485–488 (2011).

26. McKee, T. B., Doesken, N. J., Kleist, J. *et al.* The relationship of drought frequency and duration to time scales. In *Proceedings of the 8th Conference on Applied Climatology*, vol. 17, 179–183 (Boston, 1993).

27. TRMM (TMPA/3B43) Rainfall Estimate L3 1 Month 0.25 Degree× 0.25 Degree V7 Version, Greenbelt, MD, Goddard Earth Sciences Data and Information Services Center (GES DISC). https://disc.gsfc.nasa.gov/datasets/TRMM_3B43_7/summary. Accessed: 2020-10-10.

28. Bojinski, S. *et al.* The concept of essential climate variables in support of climate research, applications, and policy. *Bull. Am. Meteorol. Soc.* **95**, 1431–1443 (2014).

29. Mpelasoka, F., Hennessy, K., Jones, R. & Bates, B. Comparison of suitable drought indices for climate change impacts assessment over australia towards resource management. *Int. J. Climatol.* **28**, 1283–1292, DOI: 10.1002/joc.1649 (2008).

30. Le Page, M. & Zribi, M. Analysis and predictability of drought in northwest africa using optical and microwave satellite remote sensing products. *Sci. reports* **9**, 1–13 (2019).

31. Lopez, T., Al Bitar, A., Biancamaria, S., Güntner, A. & Jäggi, A. On the use of satellite remote sensing to detect floods and droughts at large scales. *Surv. Geophys.* **41**, 1461–1487 (2020).

32. Bouras, E. *et al.* Linkages between rainfed cereal production and agricultural drought through remote sensing indices and a land data assimilation system: a case study in morocco. *Remote. Sens.* **12**, 4018 (2020).

33. Wan, Z. New refinements and validation of the modis land-surface temperature/emissivity products. *Remote. sensing Environ.* **112**, 59–74 (2008).

34. Gu, Y., Brown, J. F., Verdin, J. P. & Wardlow, B. A five-year analysis of modis ndvi and ndwi for grassland drought assessment over the central great plains of the united states. *Geophys. research letters* **34** (2007).

35. Unganai, L. S. & Kogan, F. N. Drought monitoring and corn yield estimation in southern africa from avhrr data. *Remote. sensing environment* **63**, 219–232 (1998).

36. Kogan, F. N. Application of vegetation index and brightness temperature for drought detection. *Adv. space research* **15**, 91–100 (1995).

37. Mishra, A. K. & Singh, V. P. A review of drought concepts. *J. Hydrol.* **391**, 202 – 216, DOI: https://doi.org/10.1016/j.jhydrol.2010.07.012 (2010).

38. Vicente-Serrano, S. M., Beguería, S. & López-Moreno, J. I. A multiscalar drought index sensitive to global warming: the standardized precipitation evapotranspiration index. *J. climate* **23**, 1696–1718 (2010).

39. Palmer, W. C. *Meteorological drought*, vol. 30 (US Department of Commerce, Weather Bureau, 1965).

40. Guttman, N. B. Comparing the palmer drought index and the standardized precipitation index1. *JAWRA J. Am. Water Resour. Assoc.* **34**, 113–121, DOI: 10.1111/j.1752-1688.1998.tb05964.x (1998). https://onlinelibrary.wiley.com/doi/pdf/10.1111/j.1752-1688.1998.tb05964.x.

41. Dai, A., Trenberth, K. E. & Qian, T. A Global Dataset of Palmer Drought Severity Index for 1870–2002: Relationship with Soil Moisture and Effects of Surface Warming. *J. Hydrometeorol.* **5**, 1117–1130, DOI: 10.1175/JHM-386.1 (2004). https://journals.ametsoc.org/jhm/article-pdf/5/6/1117/4155742/jhm-386_1.pdf.

42. Hoffmann, D., Gallant, A. J. & Arblaster, J. M. Uncertainties in drought from index and data selection. *J. Geophys. Res. Atmospheres* **125**, e2019JD031946 (2020).

43. Yves, T. *et al.* Challenges for drought assessment in the mediterranean region under future climate scenarios. *Earth-Science Rev.* 103348 (2020).

44. Hersbach, H. *et al.* The era5 global reanalysis. *Q. J. Royal Meteorol. Soc.* **146**, 1999–2049 (2020).

45. Haiden, T. *et al.* Use of in situ surface observations at ECMWF. https://www.ecmwf.int/sites/default/files/elibrary/2018/18748-use-situ-surface-observations-ecmwf.pdf (2018). Accessed: 2020-10-10.

46. Ulaby, F., Moore, R. & Fung, A. *Microwave Remote Sensing: Active and Passive*. Artech House remote sensing library (Artech House, 1986).

47. Draper, D. W. & de Matthaeis, P. Radio frequency interference trends for the amsr-e and amsr2 radiometers. In *IGARSS 2018 - 2018 IEEE International Geoscience and Remote Sensing Symposium*, 301–304, DOI: 10.1109/IGARSS.2018.8518061 (2018).

48. Beck, H. E. *et al.* Global-scale evaluation of 22 precipitation datasets using gauge observations and hydrological modeling. *Hydrol. Earth Syst. Sci.* **21**, 6201–6217, DOI: 10.5194/hess-21-6201-2017 (2017).

49. Nashwan, M. S., Shahid, S. & Wang, X. Assessment of satellite-based precipitation measurement products over the hot desert climate of egypt. *Remote. sensing* **11**, 555 (2019).

50. Liu, Y., Liu, Y. & Wang, W. Inter-comparison of satellite-retrieved and global land data assimilation system-simulated soil moisture datasets for global drought analysis. *Remote. Sens. Environ.* **220**, 1 – 18, DOI: https://doi.org/10.1016/j.rse.2018.10.026 (2019).

51. Svoboda, M., Hayes, M. & Wood, D. Standardized precipitation index user guide. https://library.wmo.int/index.php?lvl=notice_display&id=13682 (2012). Accessed: 2020-10-10.

52. Spinoni, J. *et al.* A new global database of meteorological drought events from 1951 to 2016. *J. Hydrol. Reg. Stud.* **22**, 100593, DOI: https://doi.org/10.1016/j.ejrh.2019.100593 (2019).

53. Mathbout, S., Lopez-Bustins, J. A., Martin-Vide, J., Bech, J. & Rodrigo, F. S. Spatial and temporal analysis of drought variability at several time scales in syria during 1961–2012. *Atmospheric Res.* **200**, 153–168 (2018).

54. Hssaisoune, M., Bouchaou, L., Sifeddine, A., Bouimetarhan, I. & Chehbouni, A. Moroccan groundwater resources and evolution with global climate changes. *Geosciences* **10**, 81 (2020).

55. Fakir, Y. *et al.* Multi-modeling assessment of recent changes in groundwater resource: application to the semi-arid haouz plain (central morocco). *EGUGA* 14624 (2015).

56. ICARDA. ICARDA Annual Report 2003. https://www.icarda.org/publications/6284/icarda-annual-report-2003 (2003). Accessed: 2020-10-10.

57. Aw-Hassan, A., Rida, F., Telleria, R. & Bruggeman, A. The impact of food and agricultural policies on groundwater use in syria. *J. Hydrol.* **513**, 204 – 215, DOI: https://doi.org/10.1016/j.jhydrol.2014.03.043 (2014).

58. Le Page, M. *et al.* Projection of irrigation water demand based on the simulation of synthetic crop coefficients and climate change. *Hydrol. Earth Syst. Sci. Discuss.* **2020**, 1–24, DOI: 10.5194/hess-2020-301 (2020).

59. Boudhar, A. *et al.* Evaluation of the snowmelt runoff model in the moroccan high atlas mountains using two snow-cover estimates. *Hydrol. sciences journal* **54**, 1094–1113 (2009).

60. Jarlan, L. *et al.* Remote sensing of water resources in semi-arid mediterranean areas: The joint international laboratory trema. *Int. J. Remote. Sens.* **36**, 4879–4917 (2015).

61. Food and Agriculture Organization of the United Nations. Fundamental shift in drought management needed in near east and north africa region. https://https://cutt.ly/CgKdTGO (2014). Accessed: 2020-10-10.

62. Ahmed, S. M. Impacts of drought, food security policy and climate change on performance of irrigation schemes in sub-saharan africa: The case of sudan. *Agric. Water Manag.* **232**, 106064, DOI: https://doi.org/10.1016/j.agwat.2020.106064 (2020).

63. Zhang, Y., Block, P., Hammond, M. & King, A. Ethiopia's grand renaissance dam: Implications for downstream riparian countries. *J. Water Resour. Plan. Manag.* **141**, 05015002 (2015).

64. World Health Organization. UN-water global analysis and assessment of sanitation and drinking-water (GLAAS) 2014 report: investing in water and sanitation: increasing access, reducing inequalities. https://www.who.int/water_sanitation_health/publications/glaas_report_2014/en/ (2014). Accessed: 2020-10-10.

65. World Bank. Making the most of scarcity: Accountability for better water management results in the middle east and north africa. https://data.worldbank.org/region/middle-east-and-north-africa (2007). Accessed: 2020-10-10.

66. World Bank. The World Bank MENA stats 2019. https://data.worldbank.org/region/middle-east-and-north-africa (2019). Accessed: 2020-10-10.

67. Jarlan, L. *et al.* Linkages between common wheat yields and climate in morocco (1982–2008). *Int. journal biometeorology* **58**, 1489–1502 (2014).

68. López-Moreno, J. *et al.* Effects of the north atlantic oscillation (nao) on combined temperature and precipitation winter modes in the mediterranean mountains: Observed relationships and projections for the 21st century. *Glob. Planet. Chang.* **77**, 62 – 76, DOI: https://doi.org/10.1016/j.gloplacha.2011.03.003 (2011).

69. Hijmans, R. and others. Global Administrative Areas Database *GADM*, *version*4.3, 2018. http://www.gadm.org (2018). Accessed: 2020-10-10.

70. Bazza, M., Kay, M., Knutson, C. *et al.* Drought characteristics and management in North Africa and the Near East. *FAO Water Reports* (2018).

71. Verner, D. *et al. Climate Variability, Drought, and Drought Management in Morocco's Agricultural Sector* (World Bank, 2018).

72. Lück, A. *et al.* Integrated Drought Risk Management - DRM Iraq. https://reliefweb.int/sites/reliefweb.int/files/resources/Droughtexecutivesummary.pdf (2014). Accessed: 2020-10-10.

73. Tamer, A., N Abd-Aal & Abd-El-Rahman, H. Drought condition and management strategies in Egypt. https://www.droughtmanagement.info/literature/UNW-DPC_NDMP_Country_Report_Egypt_2014.pdf (2014). Accessed: 2020-10-10.

74. Yagoub, Y. E. *et al.* Detection of drought cycles pattern in two countries (Sudan and South Sudan) by using standardized precipitation index SPI. *Am J Environ Eng* **7**, 93–105 (2017).

75. Gaznayee, H. & Al-Quraishi, A. Identifying Drought Status in Duhok Governorate (Iraqi Kurdistan Region) from 1998 through 2012 using Landsat Time Series Dataset. *J. Appl. Sci. Technol. Trends* **1**, 17–23 (2020).

76. Telesca, L., Shaban, A. & Awad, M. Analysis of heterogeneity of aridity index periodicity over Lebanon. *Acta Geophys.* **67**, 167–176 (2019).

77. Salah, Z., Nieto, R., Drumond, A., Gimeno, L. & Vicente-Serrano, S. M. A Lagrangian analysis of the moisture budget over the Fertile Crescent during two intense drought episodes. *J. Hydrol.* **560**, 382–395 (2018).

78. Almazroui, M. Assessment of meteorological droughts over Saudi Arabia using surface rainfall observations during the period 1978–2017. *Arab. J. Geosci.* **12**, 694 (2019).

79. Almedeij, J. Drought analysis for Kuwait using standardized precipitation index. *The Sci. World J.* **2014** (2014).

80. Al-Ajmi, D. Climate aridity: the Sultanate of Oman as a case study. *Int J Earth Sci Geol* **1**, 1–3 (2018).

81. Yacoub, E. & Tayfur, G. Spatial and temporal of variation of meteorological drought and precipitation trend analysis over whole Mauritania. *J. Afr. Earth Sci.* **163**, 103761 (2020).

82. Ryan, K. Drought and conflict leave 8.7 million people hungry in Somalia and South Sudan. https://reliefweb.int/report/south-sudan/drought-and-conflict-leave-87-million-people-hungry-somalia-and-south-sudan (2019). Accessed: 2020-10-10.

83. International Federation's Disaster Relief Emergency Fund. DREF operation MDRSY001 GLIDE DR-2009-000149-SYR. https://reliefweb.int/report/south-sudan/drought-and-conflict-leave-87-million-people-hungry-somalia-and-south-sudan (2009). Accessed: 2020-10-10.

84. Lund, A. Drought, corruption, and war: Syria's agricultural crisis. https://carnegie-mec.org/diwan/55376 (2014). Accessed: 2020-10-10.

85. Guha-Sapir, D., Below, R. & Hoyois, P. EM-dat: the OFDA/CRED international disaster database. https://www.em-dat.be (2014). Accessed: 2020-10-10.

86. JRC. Drought worsens conflict-driven food security crisis in Yemen: Below-average summer crop production in Iraq and parts of central Asia. https://ec.europa.eu/jrc/en/science-update/drought-worsens-conflict-driven-food-security-crisis-yemen-below-average-summer-crop-production-iraq (2018). Accessed: 2020-10-10.

87. Huffman, G. J. *et al.* The TRMM multisatellite precipitation analysis (TMPA): Quasi-global, multiyear, combined-sensor precipitation estimates at fine scales. *J. hydrometeorology* **8**, 38–55 (2007).

88. Dorigo, W. *et al.* ESA CCI Soil Moisture for improved Earth system understanding: State-of-the art and future directions. *Remote. Sens. Environ.* **203**, 185–215 (2017).

89. Dee, D. P. *et al.* The ERA-Interim reanalysis: configuration and performance of the data assimilation system. *Q. J. Royal Meteorol. Soc.* **137**, 553–597, DOI: 10.1002/qj.828 (2011). https://rmets.onlinelibrary.wiley.com/doi/pdf/10.1002/qj.828.

90. Hennermann, K. & Berrisford, P. What are the changes from ERA-Interim to ERA5 (2018). Accessed: 2020-10-10.

91. Theia Hydroweb Series Temporelles de hauteurs d'eau sur les fleuves et lacs du monde. http://hydroweb.theia-land.fr/. Accessed: 2020-10-10.

92. Da Silva, J. S. *et al.* Water levels in the amazon basin derived from the ers 2 and envisat radar altimetry missions. *Remote. sensing environment* **114**, 2160–2181 (2010).

93. Crétaux, J.-F. *et al.* Sols: A lake database to monitor in the near real time water level and storage variations from remote sensing data. *Adv. space research* **47**, 1497–1507 (2011).

94. Zarch, M. A. A., Sivakumar, B. & Sharma, A. Droughts in a warming climate: A global assessment of standardized precipitation index (spi) and reconnaissance drought index (rdi). *J. Hydrol.* **526**, 183–195 (2015).

95. Heim, J., Richard R. A Review of Twentieth-Century Drought Indices Used in the United States. *Bull. Am. Meteorol. Soc.* **83**, 1149–1166, DOI: 10.1175/1520-0477-83.8.1149 (2002). https://journals.ametsoc.org/bams/article-pdf/83/8/1149/3733591/1520-0477-83_8_1149.pdf.

Acknowledgements

This study was financed by the ERANET3-062 CHAAMS project and the GRDI O'LIFE from the "Centre National de Recherche Scientifique" (CNRS) of France and the "Centre National de Recherche Scientifique Liban" (CNRS-L). Additional funding was provided by the MISTRAL/SICMED2 program. The co-authors thank the European Space Agency (ESA) Climate Change Initiative (CCI), the National Aeronautics and Space Administration (NASA) US, and the European Centre for Medium Range Weather Forecast (ECMWF) for the data availability of the soil moisture and precipitation datasets.

Author contributions statement

A.A. conceived the experiment(s), A.A. and S.N. conducted the experiment(s), A.A. and S.N. analysed the results, A.A. prepared the original manuscript. All authors reviewed the manuscript.

Competing interests All authors declare no conflicts of interest.

Figures

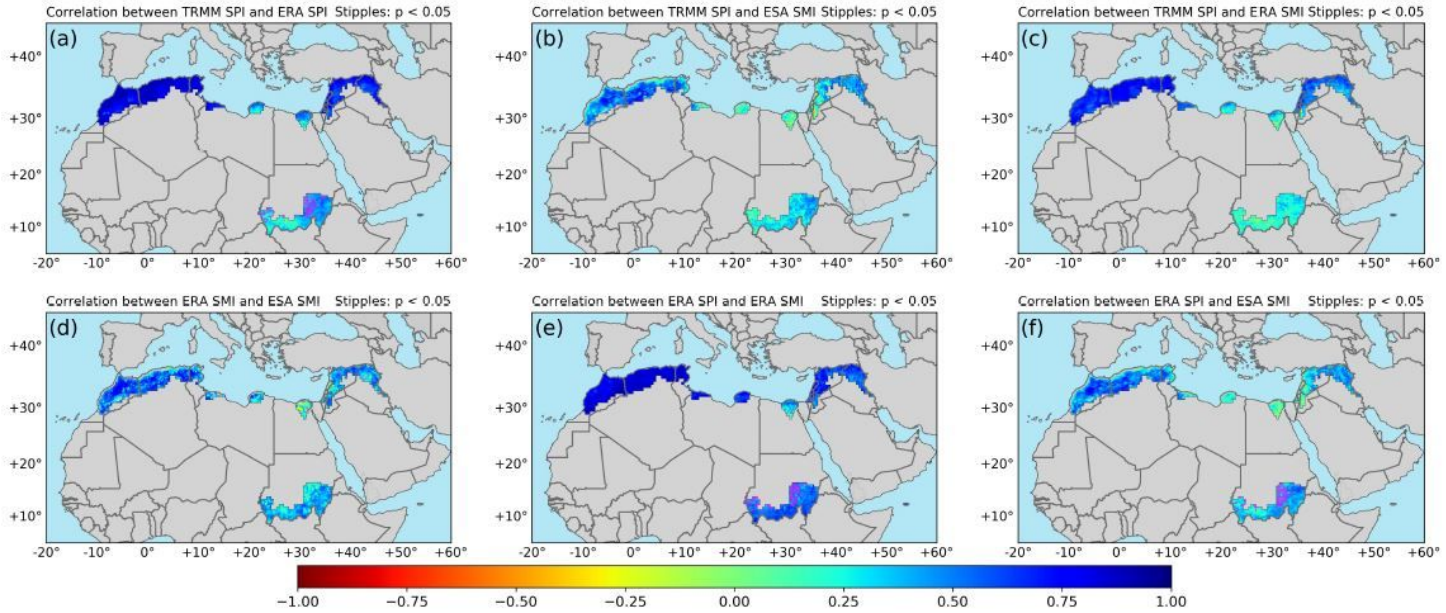

Figure 1

Pearson temporal cross-correlation maps for the four considered drought indices: Corr(TRMM SPI, ERA SPI) (a), Corr(TRMM SPI, ESA SMI) (b), Corr(TRMM SPI, ERA SMI) (c), Corr(ERA SPI, ESA SMI) (d), Corr(ERA SPI, ERA SMI) (e), and Corr(ERA SPI, ESA SMI) (f). Note: The designations employed and the presentation of the material on this map do not imply the expression of any opinion whatsoever on the part of Research Square concerning the legal status of any country, territory, city or area or of its authorities, or concerning the delimitation of its frontiers or boundaries. This map has been provided by the authors.

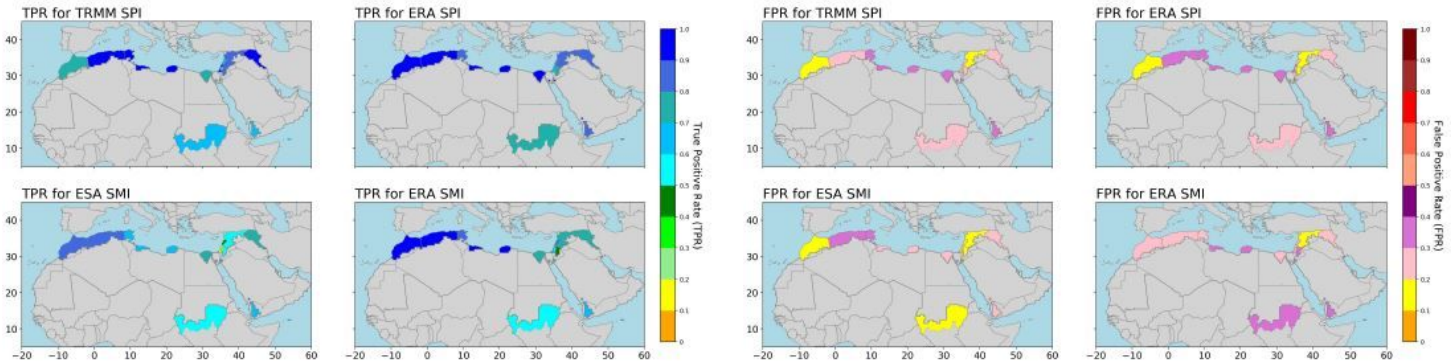

Figure 2

True positive rate (TPR) (left) and false positive rate (FPR) (right) for the TRMM SPI, ERA SPI, ESA SMI, and ERA SMI drought indices against the constructed drought database. Note: The designations employed and the presentation of the material on this map do not imply the expression of any opinion

whatsoever on the part of Research Square concerning the legal status of any country, territory, city or area or of its authorities, or concerning the delimitation of its frontiers or boundaries. This map has been provided by the authors.

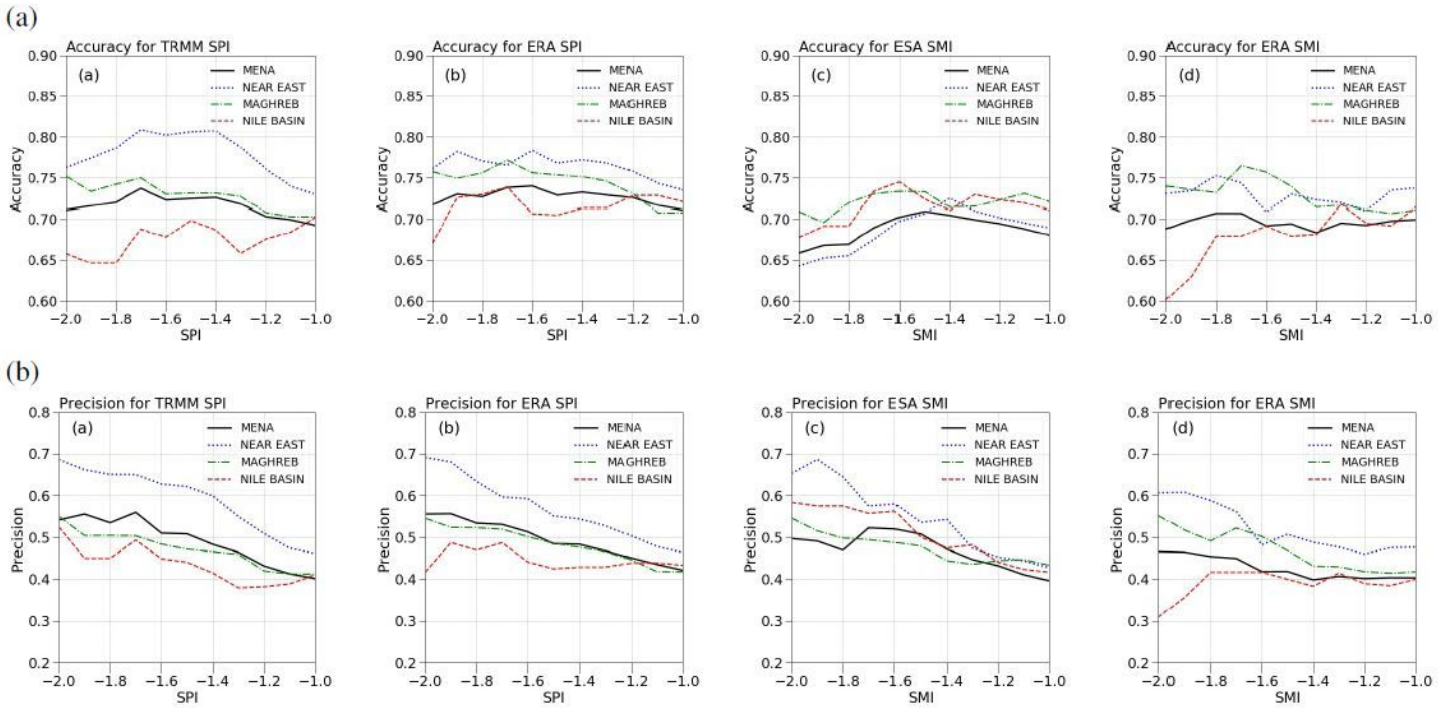

Figure 3

Accuracy and precision of the TRMM SPI, ESA SMI, ERA SPI, and ERA SMI with respect to the constructed drought dataset.

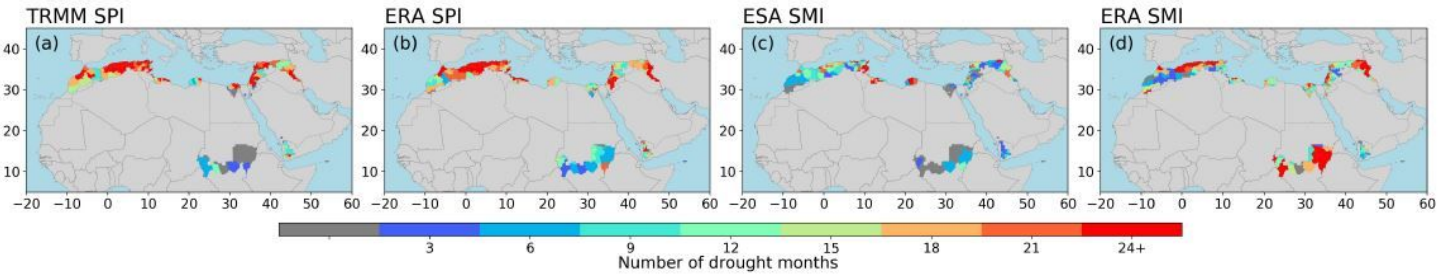

Figure 4

Number of months with severe to extreme drought events (index < -1.5) from 1998-2018 at administrative level 1 across the MENA region, from the TRMM SPI (a), ERA SPI (b), ESA SMI (c), and ERA SMI (d). Note: The designations employed and the presentation of the material on this map do not imply the expression of any opinion whatsoever on the part of Research Square concerning the legal status of any country, territory, city or area or of its authorities, or concerning the delimitation of its frontiers or boundaries. This map has been provided by the authors.

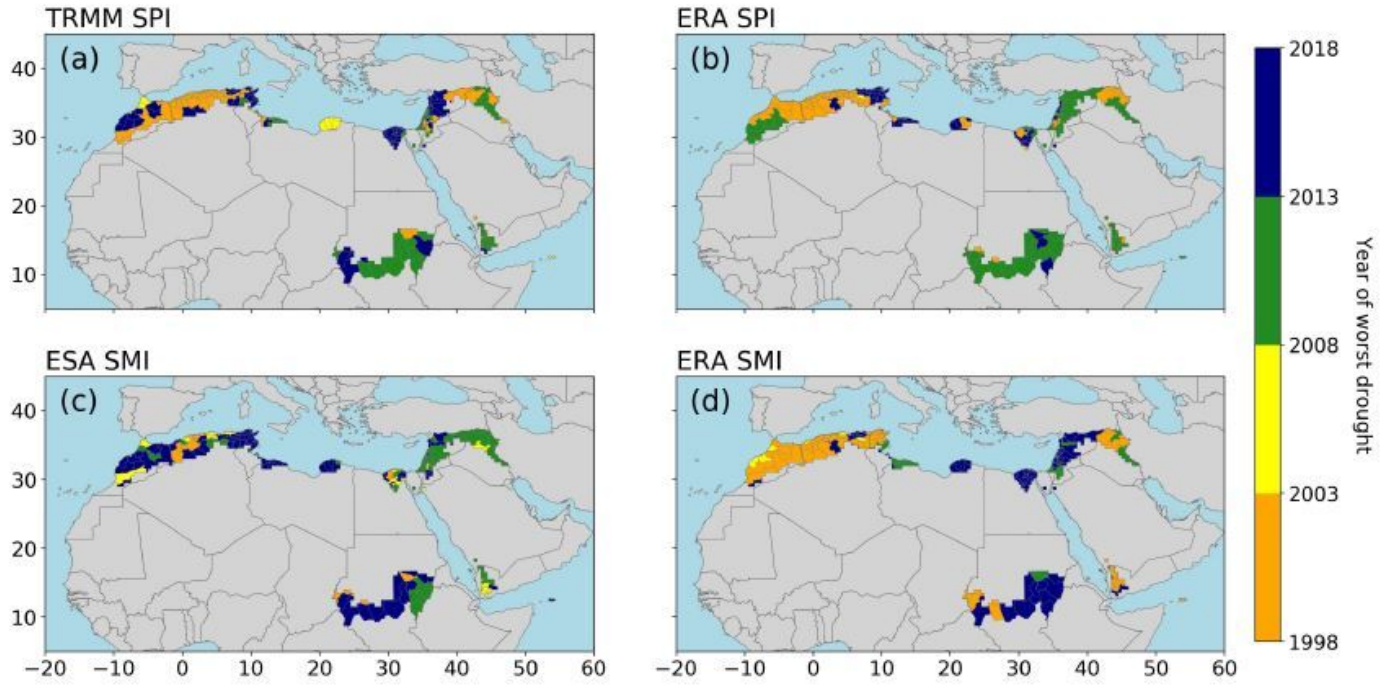

Figure 5

Period of most extreme drought by class for the 5 years from 1998-2018 for the TRMM SPI, ERA SPI, ESA SMI and ERA SMI for each column. Note: The designations employed and the presentation of the material on this map do not imply the expression of any opinion whatsoever on the part of Research Square concerning the legal status of any country, territory, city or area or of its authorities, or concerning the delimitation of its frontiers or boundaries. This map has been provided by the authors.

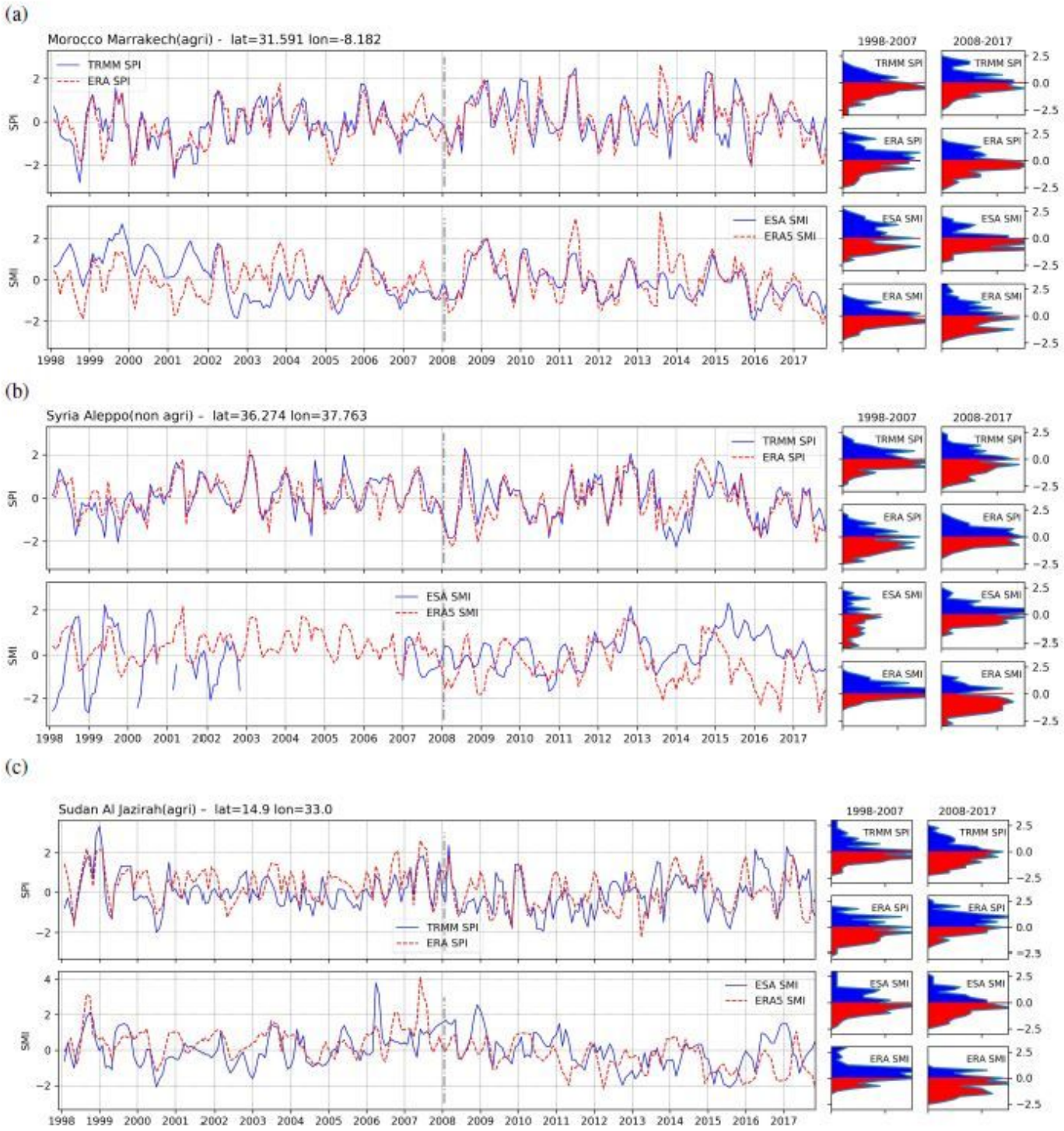

Figure 6

Time series (left) and histogram (right) of the SPI and SMI for Marrakech in Morocco, Aleppo in Syria, and Al Jazirah in Sudan. The histograms are divided into two decades for each of the four datasets.

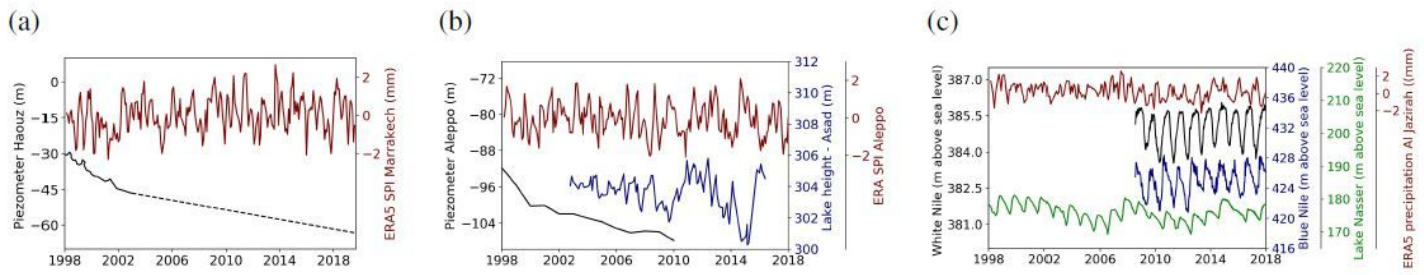

Figure 7

Time series of soil moisture from the ERA SPI and water levels of rivers, lakes and groundwater. (a) Haouz Plain, Morocco: groundwater level from54 until 2002 (Hydraulic Agency) and extrapolated to 2019 by considering a constant rate of 1 m/year based on55, (b) Aleppo, Syria: groundwater level from56, 57, and (c) Al Jazirah: White Nile, Blue Nile and Lake Nasser levels.

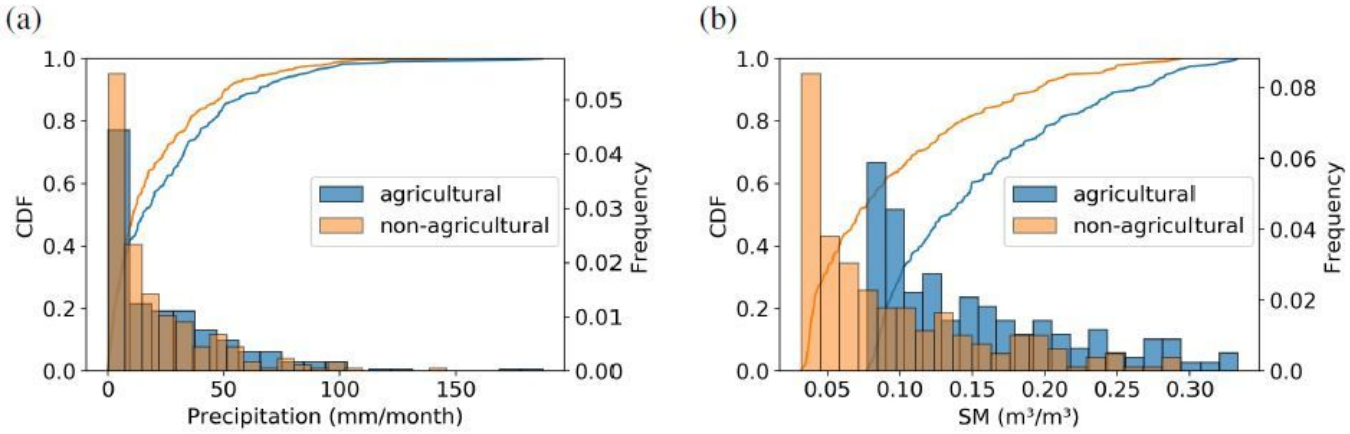

Figure 8

Statistical distribution of precipitation and soil moisture from ERA5 over agricultural and adjacent non-agricultural nodes in the Haouz Plain, Morocco.